# Electrical switching of valley polarization in monolayer semiconductors

Lizhong Li <sup>1</sup>, Shengwei Jiang <sup>2</sup>, Zefang Wang <sup>1</sup>, Kenji Watanabe <sup>3</sup>, Takashi Taniguchi <sup>3</sup>, Jie Shan <sup>1,2,4\*</sup>, and Kin Fai Mak <sup>1,2,4#</sup>

School of Applied and Engineering Physics, Cornell University, Ithaca, New York
 Department of Physics, Cornell University, Ithaca, New York
 National Institute for Materials Science, 1-1 Namiki, 305-0044 Tsukuba, Japan
 Kavli Institute at Cornell for Nanoscale Science, Ithaca, New York
 \*jie.shan@cornell.edu
 #kinfai.mak@cornell.edu

### <u>Abstract</u>

Achieving on-demand control of the valley degree of freedom is essential for valley-based information science and technology. Optical and magnetic control of the valley degree of freedom in monolayer transition metal dichalcogenide (TMD) semiconductors has been extensively studied. However, electrical control of the valley polarization has remained a challenge. Here we demonstrate switching of the valley polarization in monolayer WSe<sub>2</sub> by electrical gating. This is achieved by coupling a WSe<sub>2</sub> monolayer to a two-dimensional (2D) layered magnetic insulator CrI<sub>3</sub>. The valley degeneracy in WSe<sub>2</sub> is lifted by the magnetic proximity effect. The valley polarization is switched through gate control of the interlayer spin-flip transition in 2D CrI<sub>3</sub>, which switches the magnetization of the CrI<sub>3</sub> layer adjacent to the WSe<sub>2</sub> layer. The effect is manifested by a sign change in the photoluminescence handedness of WSe<sub>2</sub>. Our results provide the basis for high-speed and energy-efficient gate control of the valley degree of freedom in monolayer TMD semiconductors.

Monolayer transition metal dichalcogenide (TMD) semiconductors are direct band gap semiconductors with two degenerate copies of conduction and valence bands located at the K and the K' points of the Brillouin zone [1–4]. As a result of the finite and opposing Berry curvatures at the two valleys, the valley degree of freedom can be readily controlled by the optical and magnetic fields [5-17]. However, electrical control of the valley degree of freedom is essential for high-speed and energy-efficient applications. For instance, electrical control of the valley polarization (a population difference between the K and K' valleys) could enable fast and energy-efficient valley-based photonic and optoelectronic devices that encode information in the light handedness. Electrical generation of the valley magnetization in monolayer TMD semiconductors has been achieved via the valley magnetoelectric effect [18], but the effect does not generate net valley polarization [19]. Electrical control of the valley polarization has remained an experimental challenge because the valley polarization does not directly couple to an electric field.

The recent discovery of two-dimensional (2D) layered magnetic materials [20–29] and the demonstration of electrical switching of the magnetization in these materials [30–33] provide a route to realize this goal. Of particular interest in this study is few-layer CrI<sub>3</sub>, which is an A-type antiferromagnet with ferromagnetic (FM) monolayers coupled to each other with antiferromagnetic (AF) interactions [21,24,27,28,29]. Because of the weak interlayer AF exchange, an external magnetic field of less than 1 T is sufficient to induce an AF-FM spin-flip transition. The spin-flip transition field can also be efficiently tuned by electrical gating [30–32], which allows robust and repeatable switching of the material between the AF and the FM states. Electrical control of the valley polarization in monolayer TMD semiconductors is therefore possible via magnetic proximity coupling to the magnetic materials [34,35].

In this letter, we demonstrate robust and repeatable electrical switching of the valley polarization in monolayer WSe<sub>2</sub>. This is achieved by coupling the material to 2D CrI<sub>3</sub>, which lifts the valley degeneracy in WSe<sub>2</sub> by the magnetic proximity effect at the WSe<sub>2</sub>-CrI<sub>3</sub> interface [34]. Such device platform has also been employed by a recent experiment to detect the spin state of the interfacial CrI<sub>3</sub> layer [36]. By controlling the spin-flip transition with a gate voltage under a constant magnetic field, we demonstrate electrical switching of the valley polarization in WSe<sub>2</sub>, as manifested by a sign change in the photoluminescence (PL) handedness. When WSe<sub>2</sub> is coupled to a CrI<sub>3</sub> bilayer, deterministic electrical switching of the valley polarization depends on whether the CrI<sub>3</sub> layer adjacent to WSe<sub>2</sub> is a magnetic soft or magnetic hard layer. Electrical switching of the valley polarization is not repeatable for the latter. We achieve deterministic valley switching by employing 4-layer CrI<sub>3</sub>, in which repeatable electrical switching of the magnetization of the interfacial CrI<sub>3</sub> layer can be guaranteed by the exchange bias field from the interior layers.

We fabricate dual-gate field-effect devices of coupled WSe<sub>2</sub>-CrI<sub>3</sub> heterostructures (Fig. 1a and 1b) using the layer-by-layer dry transfer technique detailed elsewhere [37]. Since 2D CrI<sub>3</sub> easily degrades under ambient conditions, the devices are fabricated in a nitrogen-filled glove box with oxygen and water levels below 1 ppm. The magnetization

of CrI<sub>3</sub> is probed by the magnetic circular dichroism (MCD). The sample is illuminated by circularly polarized light centered at 633 nm. The incident light helicity is modulated by a photoelastic modulator and the difference between the left- and right-handed reflection, which is proportional to the sample magnetization, is recorded at varying magnetic fields and gate voltages. To probe the spontaneous valley polarization, the WSe<sub>2</sub> layer is excited by linearly polarized light centered at 633 nm so that the two valleys are equally excited. Handedness-resolved PL from the fundamental exciton resonance is measured by a charge-coupled device (CCD). The PL handedness  $\rho$ , defined as the difference between the left- and right-handed PL intensity divided by the total intensity, is proportional to the valley polarization [3,4]. All results presented below are obtained at 4 K.

Figure 1c shows the top gate voltage ( $V_{TG}$ ) dependence of the PL spectrum from WSe<sub>2</sub>. The WSe<sub>2</sub> layer is hole-doped when coupled to CrI<sub>3</sub>. The PL from the positively charged exciton is seen at  $V_{TG} = 0$  V. The neutral exciton PL is only seen at large positive  $V_{TG}$ 's, where the material becomes charge neutral. As a result of the large quantum capacitance of CrI<sub>3</sub>, the bottom gate voltage ( $V_{BG}$ ) has a negligible effect on the WSe<sub>2</sub> PL spectrum (Supplementary Fig. S1 and S2). Therefore, the top and bottom gate independently vary the doping level in the WSe<sub>2</sub> and the CrI<sub>3</sub> layer, respectively. The modification of the spin-flip transition field in bilayer CrI<sub>3</sub> by  $V_{BG}$  is shown by the magnetic-field dependent MCD in Fig. 1d. The material undergoes a spin-flip transition from an AF state to a fully spin-polarized state at ~ 0.8 T at  $V_{BG} = 0$  V. The spin-flip transition field decreases to ~ 0.5 T at  $V_{BG} = 9$  V. The result is consistent with earlier reports on doping-induced modifications of the spin-flip transition field in 2D CrI<sub>3</sub> [30,31]. This forms the basis for electrical switching of the valley polarization in our heterostructures.

Figure 2a shows the handedness-resolved PL spectra from WSe<sub>2</sub> at zero gate voltage and zero magnetic field. The significant difference in the left- and right-handed emission intensity and the presence of a finite Zeeman splitting of ~ 2.5 meV demonstrate the presence of strong magnetic proximity coupling at the WSe<sub>2</sub>-CrI<sub>3</sub> interface (which lifts the valley degeneracy). The finite valley splitting disappears above the critical temperature of CrI<sub>3</sub>, which further confirms the interpretation. Based on the measured Zeeman splitting and the known exciton g-factor of WSe<sub>2</sub> ( $|g| \approx 4$ ), an exchange magnetic field of  $\sim 10$  T is estimated, which is also consistent with recent reports [34]. The magnetic-field dependence of the spectrally integrated PL handedness  $\rho$  and the exciton Zeeman splitting  $\Delta$  is shown in Fig. 2b. The exciton Zeeman splitting is determined by fitting the PL spectra to Voigt functions. A clear hysteresis loop with transition fields corresponding to the spin-flip transition fields of bilayer CrI<sub>3</sub> is seen. Both the PL handedness and the exciton Zeeman splitting follow the magnetic state of the CrI<sub>3</sub> layer adjacent to WSe<sub>2</sub> and are insensitive to the magnetic state of the other CrI<sub>3</sub> layer. This is expected for magnetic proximity coupling at the WSe<sub>2</sub>-CrI<sub>3</sub> interface which is a short-range interaction.

With the demonstrated magnetic proximity coupling and the gate tunable spin-flip transition field in bilayer CrI<sub>3</sub>, the PL handedness (and therefore the valley polarization)

can now be electrically switched by switching the magnetic state of the CrI<sub>3</sub> layer adjacent to WSe<sub>2</sub>. This is demonstrated in Fig. 2c. The top panel shows the sequence of  $V_{BG}$  as a function of scanning step; and the bottom panel is the corresponding PL handedness under a constant magnetic bias of 0.9 T. Repeatable switching of the PL handedness corresponding to the gate-induced spin-flip transition is seen. The repeatability is further demonstrated in Fig. 2d, which shows switching for 30 cycles.

Although electrical switching of the valley polarization is demonstrated in Fig. 2 for WSe<sub>2</sub> coupled to bilayer CrI<sub>3</sub>, deterministic switching is not guaranteed because the WSe<sub>2</sub> layer is randomly coupled to the magnetic hard or the magnetic soft CrI<sub>3</sub> layer (the two CrI<sub>3</sub> layers are never identical). The distinctive behaviors for the two different kinds of samples are illustrated in Fig. 3a and 3b, which show the dependence of the WSe<sub>2</sub> PL handedness on magnetic field near the positive spin-flip transition field. For samples with WSe<sub>2</sub> coupled to the magnetic soft CrI<sub>3</sub> layer (Fig. 3b), which has a lower energy barrier for magnetization reorientation, the PL handedness can be switched back at the spin-flip transition after the sample magnetization is saturated at large positive fields (1.1 T). Repeatable electrical switching of the valley polarization via gate-induced spin-flip transition is therefore possible. However, when WSe<sub>2</sub> is coupled to the magnetic hard CrI<sub>3</sub> layer (Fig. 3a), which has a higher energy barrier for magnetization reorientation, the PL handedness can only be switched once at the spin-flip transition when the magnetic field increases. It cannot be switched back by decreasing the magnetic field because the magnetization of the hard layer stays unaltered after the first switch. Repeatable electrical switching of the valley polarization is thus not possible. Similar results for several other bilayer CrI<sub>3</sub> devices are shown in Supplementary Fig. S4. In addition to coupling to the magnetic hard or magnetic soft layer, signatures of coupling to both (i.e. existence of soft- and hard-domains) are seen.

To overcome this problem and to achieve deterministic valley polarization switching even if WSe<sub>2</sub> is coupled to the magnetic hard layer, we make use of the intermediate magnetic state in 4-layer CrI<sub>3</sub>. Similar to bilayer CrI<sub>3</sub>, 4-layer CrI<sub>3</sub> has an interlayer AF state under zero magnetic field (Fig. 4a). With increasing magnetic field, it undergoes two spin-flip transitions, with one at  $\sim 0.8$  T corresponding to spin-flips at the surface layers and another one at  $\sim 1.7$  T corresponding to spin-flips at the interior layer spin-flip transition field is about twice the field of the surface layers because each interior layer experiences interlayer AF exchange from two adjacent layers whereas the surface layers experience magnetic interactions only from one adjacent layer. The magnetic states of 4-layer CrI<sub>3</sub> at different magnetic fields are illustrated in Fig. 4a.

Figure 4b shows the magnetic-field dependence of the spectrally integrated PL handedness from a WSe<sub>2</sub> monolayer coupled to a 4-layer CrI<sub>3</sub> sample (see Supplementary Fig. S3 for the exciton Zeeman splitting). Similar to the case of bilayer CrI<sub>3</sub>, a clear hysteresis loop with sudden jumps between the positive and negative values of  $\rho$  at the spin-flip transitions of the surface layers is seen. The PL handedness is largely insensitive to the spin-flip transitions of the interior layers, as expected for short-range exchange coupling at the WSe<sub>2</sub>-CrI<sub>3</sub> interface. To illustrate repeatable valley polarization switching in this type of samples (Fig. 4c), we first prepare the heterostructure to the  $\downarrow\downarrow\downarrow\downarrow$ -WSe<sub>2</sub>

state (WSe<sub>2</sub> couples to the right-most CrI<sub>3</sub> layer) by sweeping the magnetic field to -2.2 T, which fully saturates the 4-layer CrI<sub>3</sub> to the spin-down state \limits\_\limits\_\limits. No significant change in the PL handedness is seen as the magnetic field increases from -2.2 T to  $\sim 0.8$ T, which induces spin-flip transitions only at the interior layers. As the sample goes through a spin-flip transition from  $\uparrow\downarrow\uparrow\downarrow$ -WSe<sub>2</sub> to  $\uparrow\downarrow\uparrow\uparrow$ -WSe<sub>2</sub> at  $\sim$  0.8 T, the PL handedness changes from  $\sim$  -20 % to  $\sim$  +20%. Now as long as the magnetic field does not exceed the second spin-flip transition that brings the sample to 111-WSe2, valley polarization switching is repeatable because the magnetic state of the interior layers, which provide an exchange bias to the surface layer, remains unchanged. Indeed, if we stop at 1.5 T and scan the field backwards, the sample goes back to 111-WSe2 from 111 1-WSe<sub>2</sub> and the PL handedness changes sign accordingly. Conversely, this is no longer the case if the magnetic field exceeds the second spin-flip transition field of  $\sim 1.7$  T. under which the magnetic state of the interior layers is modified (see Fig. 4a and 4b). In this case, repeatable valley polarization switching can only be reestablished near the spin-flip transition of the surface layers at negative magnetic field (~ -0.8 T), provided that the magnetic field does not decrease beyond the second spin-flip transition (near -1.7 T).

The intermediate magnetic state of 4-layer  $CrI_3$  has solved the magnetic soft and hard layer problem in bilayer  $CrI_3$  so that deterministic electrical switching of the valley polarization becomes possible. We first initialize the sample at the  $\uparrow\downarrow\uparrow\downarrow$ -WSe<sub>2</sub> state by polarizing it at -2.2 T followed by turning the magnetic field back to 0 T. We then magnetically bias the sample at 0.7 T near the first spin-flip transition field. Figure 4d shows the  $V_{BG}$  dependence of the PL handedness and the MCD signal under this condition. The hysteresis loop corresponds to the gate-induced spin-flip transition in 4-layer  $CrI_3$ , which switches the valley polarization via the magnetic proximity effect. Repeatable electrical switching of the PL handedness over many cycles is shown in Fig. 4e.

Finally, we note the presence of another possible configuration \$\psi\psi\-\WSe\_2\$ (in addition to \$\psi\psi\-\WSe\_2\$) after we initialize the sample at -2.2 T and turn off the magnetic field. For this configuration, the PL handedness switching shown in Fig. 4c would have occurred at -0.8 T instead of +0.8 T. To achieve repeatable electrical switching of the valley polarization in this configuration, we need to either initialize the sample at -2.2 T and magnetically bias near -0.8 T or initialize the sample at +2.2 T and magnetically bias near + 0.8 T. The situation is similar to the magnetic hard or magnetic soft layer issue in bilayer CrI<sub>3</sub> devices discussed in Fig. 3. However, unlike the bilayer CrI<sub>3</sub> devices, repeatable electrical switching of the valley polarization can be achieved in both configurations for 4-layer CrI<sub>3</sub> devices thanks to the intermediate magnetic states.

In conclusion, we have realized deterministic and repeatable electrical switching of the valley polarization of monolayer WSe<sub>2</sub> in a gated WSe<sub>2</sub>-CrI<sub>3</sub> heterostructure. This is possible thanks to the strong magnetic proximity effect at the WSe<sub>2</sub>-CrI<sub>3</sub> interface and the doping-dependent spin-flip transition field in 2D CrI<sub>3</sub>. To ensure deterministic valley switching, we make use of the intermediate magnetic states in 4-layer CrI<sub>3</sub>, in which the interior layers provide a necessary exchange bias to the surface layer. Although a

constant magnetic bias of  $\sim 1$  T is required, switching near zero magnetic field is possible by intentional electron doping of the CrI<sub>3</sub> crystals, which can substantially weaken the interlayer AF coupling [30]. The ability to switch the valley polarization by an electric field will enable high-speed and energy-efficient valley-based device concepts.

# Acknowledgements

We acknowledge support from the Air Force Office of Scientific Research under award FA9550-18-1-0480 for sample and device fabrication and the National Science Foundation under DMR-1807810 for optical measurements. This work was also partially supported by the Cornell Center for Materials Research with funding from the NSF MRSEC program (DMR-1719875) for characterization of the magnetic materials.

#### References

- [1] K. F. Mak, C. Lee, J. Hone, J. Shan, and T. F. Heinz, Physical Review Letters **105**, 136805 (2010).
- [2] A. Splendiani, L. Sun, Y. Zhang, T. Li, J. Kim, C.-Y. Chim, G. Galli, and F. Wang, Nano Letters 10, 1271 (2010).
- [3] X. Xu, W. Yao, D. Xiao, and T. F. Heinz, Nature Physics 10, 343 (2014).
- [4] K. F. Mak and J. Shan, Nature Photonics **10**, 216 (2016).
- [5] Y. P. Shkolnikov, E. P. De Poortere, E. Tutuc, and M. Shayegan, Physical Review Letters **89**, 226805 (2002).
- [6] O. Gunawan, Y. P. Shkolnikov, K. Vakili, T. Gokmen, E. P. De Poortere, and M. Shayegan, Physical Review Letters **97**, 186404 (2006).
- [7] K. F. Mak, K. He, J. Shan, and T. F. Heinz, Nature Nanotechnology 7, 494 (2012).
- [8] T. Cao, G. Wang, W. Han, H. Ye, C. Zhu, J. Shi, Q. Niu, P. Tan, E. Wang, B. Liu, and J. Feng, Nature Communications 3, 887 (2012).
- [9] H. Zeng, J. Dai, W. Yao, D. Xiao, and X. Cui, Nature Nanotechnology 7, 490 (2012).
- [10] A. M. Jones, H. Yu, N. J. Ghimire, S. Wu, G. Aivazian, J. S. Ross, B. Zhao, J. Yan, D. G. Mandrus, D. Xiao, W. Yao, and X. Xu, Nature Nanotechnology **8**, 634 (2013).
- [11] X. Li, F. Zhang, and Q. Niu, Physical Review Letters **110**, 066803 (2013).
- [12] T. Cai, S. A. Yang, X. Li, F. Zhang, J. Shi, W. Yao, and Q. Niu, Physical Review B Condensed Matter and Materials Physics 88, 115140 (2013).
- [13] K. F. Mak, K. L. McGill, J. Park, and P. L. McEuen, Science **344**, 1489 (2014).
- [14] D. Macneill, C. Heikes, K. F. Mak, Z. Anderson, A. Kormányos, V. Zólyomi, J. Park, and D. C. Ralph, (2015).
- [15] A. Srivastava, M. Sidler, A. V. Allain, D. S. Lembke, A. Kis, and A. Imamollu, Nature Physics 11, 141 (2015).

- [16] J. Lee, K. F. Mak, and J. Shan, Nature Nanotechnology 11, 421 (2016).
- [17] Z. Wang, J. Shan, and K. F. Mak, Nature Nanotechnology 12, 144 (2017).
- [18] J. Lee, Z. Wang, H. Xie, K. F. Mak, and J. Shan, Nature Materials 16, 887 (2017).
- [19] H. Yu and W. Yao, Nature Materials **16**, 876 (2017).
- [20] J. U. Lee, S. Lee, J. H. Ryoo, S. Kang, T. Y. Kim, P. Kim, C. H. Park, J. G. Park, and H. Cheong, Nano Letters **16**, 7433 (2016).
- [21] B. Huang, G. Clark, E. Navarro-Moratalla, D. R. Klein, R. Cheng, K. L. Seyler, Di. Zhong, E. Schmidgall, M. A. McGuire, D. H. Cobden, W. Yao, D. Xiao, P. Jarillo-Herrero, and X. Xu, Nature **546**, 270 (2017).
- [22] C. Gong, L. Li, Z. Li, H. Ji, A. Stern, Y. Xia, T. Cao, W. Bao, C. Wang, Y. Wang,
  Z. Q. Qiu, R. J. Cava, S. G. Louie, J. Xia, and X. Zhang, Nature 546, 265 (2017).
- [23] Y. Deng, Y. Yu, Y. Song, J. Zhang, N. Z. Wang, Z. Sun, Y. Yi, Y. Z. Wu, S. Wu, J. Zhu, J. Wang, X. H. Chen, and Y. Zhang, Nature **563**, 94 (2018).
- [24] K. S. Burch, D. Mandrus, and J. G. Park, Nature **563**, 47 (2018).
- [25] M. Bonilla, S. Kolekar, Y. Ma, H. C. Diaz, V. Kalappattil, R. Das, T. Eggers, H. R. Gutierrez, M. H. Phan, and M. Batzill, Nature Nanotechnology **13**, 289 (2018).
- [26] D. J. O'Hara, T. Zhu, A. H. Trout, A. S. Ahmed, Y. K. Luo, C. H. Lee, M. R. Brenner, S. Rajan, J. A. Gupta, D. W. McComb, and R. K. Kawakami, Nano Letters 18, 3125 (2018).
- [27] K. F. Mak, J. Shan, and D. C. Ralph, Nature Reviews Physics 1, 646 (2019).
- [28] M. Gibertini, M. Koperski, A. F. Morpurgo, and K. S. Novoselov, Nature Nanotechnology **14**, 408 (2019).
- [29] C. Gong and X. Zhang, Science 363, (2019).
- [30] S. Jiang, L. Li, Z. Wang, K. F. Mak, and J. Shan, Nature Nanotechnology 13, 549 (2018).
- [31] S. Jiang, J. Shan, and K. F. Mak, Nature Materials 17, 406 (2018).
- [32] B. Huang, G. Clark, D. R. Klein, D. MacNeill, E. Navarro-Moratalla, K. L. Seyler, N. Wilson, M. A. McGuire, D. H. Cobden, D. Xiao, W. Yao, P. Jarillo-Herrero, and X. Xu, Nature Nanotechnology **13**, 544 (2018).
- [33] Z. Wang, T. Zhang, M. Ding, B. Dong, Y. Li, M. Chen, X. Li, J. Huang, H. Wang, X. Zhao, Y. Li, D. Li, C. Jia, L. Sun, H. Guo, Y. Ye, D. Sun, Y. Chen, T. Yang, J. Zhang, S. Ono, Z. Han, and Z. Zhang, Nature Nanotechnology 13, 554 (2018).
- [34] D. Zhong, K. L. Seyler, X. Linpeng, R. Cheng, N. Sivadas, B. Huang, E. Schmidgall, T. Taniguchi, K. Watanabe, M. A. McGuire, W. Yao, D. Xiao, K. M. C. Fu, and X. Xu, Science Advances 3, e1603113 (2017).
- [35] K. L. Seyler, D. Zhong, B. Huang, X. Linpeng, N. P. Wilson, T. Taniguchi, K. Watanabe, W. Yao, D. Xiao, M. A. McGuire, K. M. C. Fu, and X. Xu, Nano Letters 18, 3823 (2018).

- [36] D. Zhong, K. L. Seyler, X. Linpeng, N. P. Wilson, T. Taniguchi, K. Watanabe, M. A. McGuire, K. M. C. Fu, D. Xiao, W. Yao, and X. Xu, Nature Nanotechnology 15, 187 (2020).
- [37] L. Wang, I. Meric, P. Y. Huang, Q. Gao, Y. Gao, H. Tran, T. Taniguchi, K. Watanabe, L. M. Campos, D. A. Muller, J. Guo, P. Kim, J. Hone, K. L. Shepard, and C. R. Dean, Science **342**, 614 (2013).

# Figures and figure captions

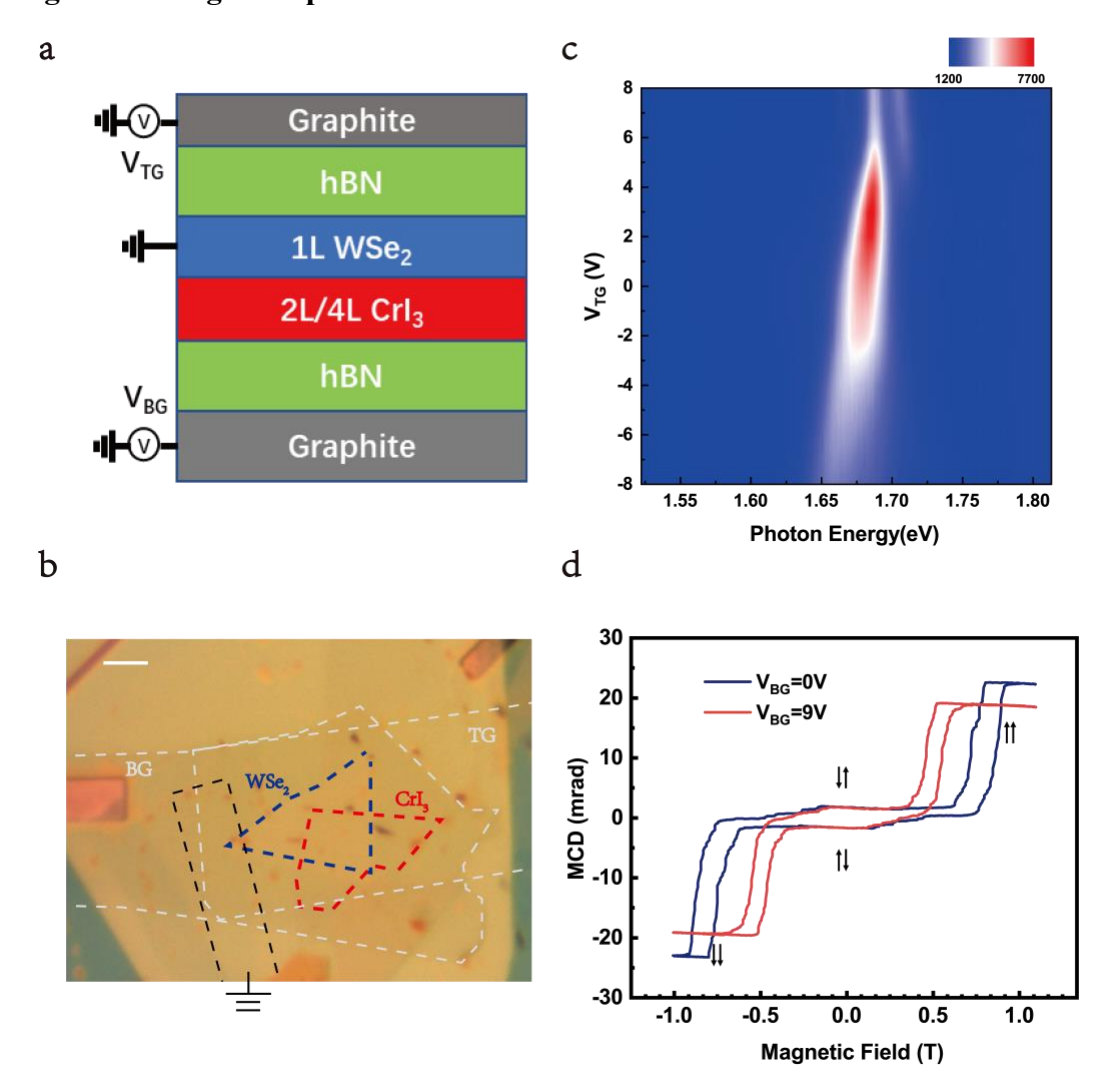


Figure 1(a) Schematic side view of a dual-gate monolayer WSe<sub>2</sub>/multilayer CrI<sub>3</sub> heterostructure. (b) Optical micrograph of a device used in this study. The WSe<sub>2</sub> (CrI<sub>3</sub>) region is outlined by the blue (red) dashed line. The top and bottom graphite gate electrodes are outlined by white dashed lines, and the graphite contact electrode (grounded) is outlined by the black dashed line. Scale bar is 5 μm. (c) The top-gate-dependent PL spectrum of the device shown in (b). The bottom gate voltage is fixed at 0 V. The WSe<sub>2</sub> layer is hole-doped due to charge transfer between the WSe<sub>2</sub> and CrI<sub>3</sub> layer. (d) MCD versus magnetic field measured on the WSe<sub>2</sub>/CrI<sub>3</sub> overlapped region at two different back gate voltages. The top gate voltage is fixed at 0 V.

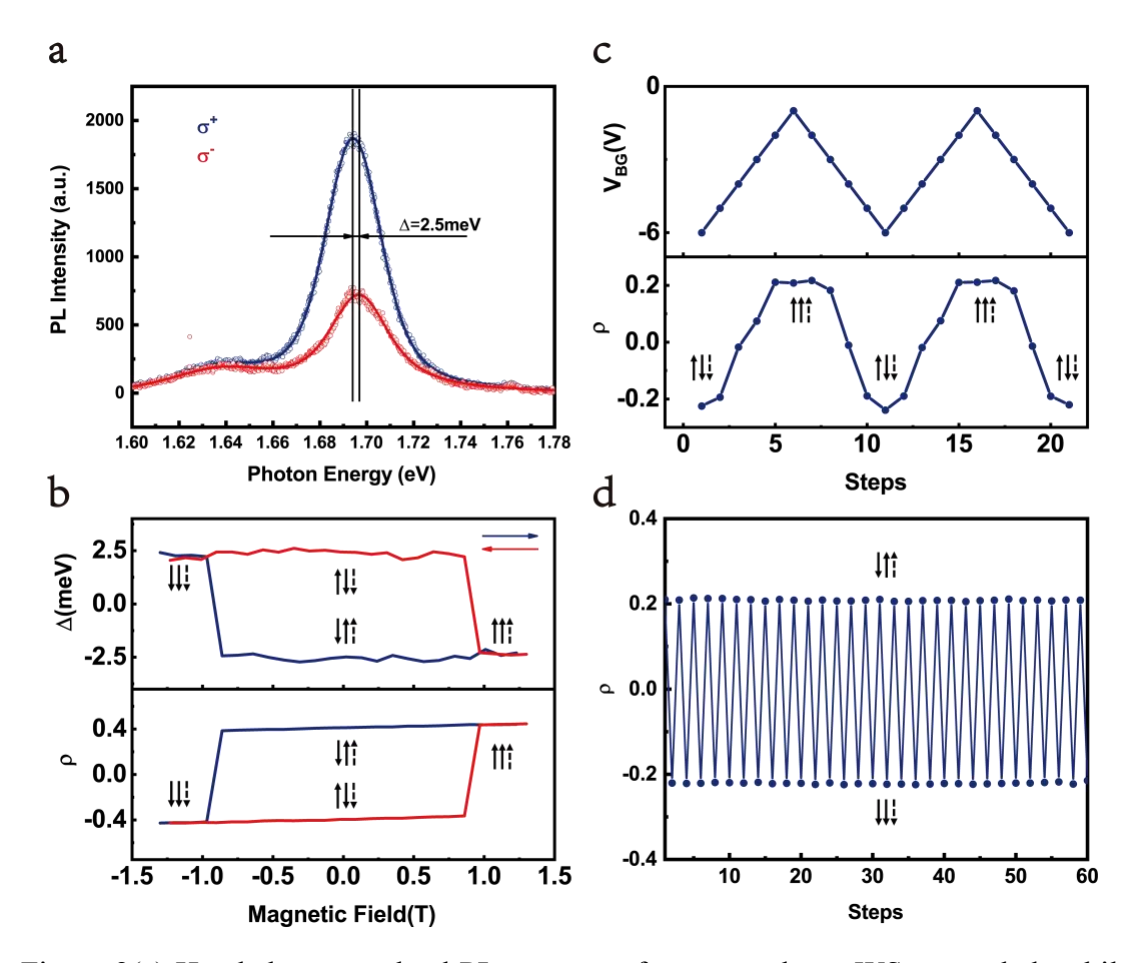


Figure 2(a) Handedness-resolved PL spectrum from monolayer WSe<sub>2</sub> coupled to bilayer CrI<sub>3</sub> at zero magnetic field. The PL spectrum for each handedness is fitted with two Voigt functions (solid lines) to account for the main peak and the weaker feature at a lower energy. Valley Zeeman splitting of 2.5 meV is extracted for the main peak. (b) Exciton Zeeman splitting  $\Delta$  (upper panel) and spectrally integrated PL handedness  $\rho$  (lower panel) as a function of magnetic field. (c) The PL handedness (lower panel) and the back-gate voltage  $V_{BG}$  (upper panel) as a function of switching step of  $V_{BG}$  under a fixed magnetic field 0.9 T and  $V_{TG} = 0$  V. (d) Electrical switching of PL handedness under the same condition as in (c) for 30 cycles as  $V_{BG}$  is switched between two values -1 V and -6 V. The spin directions of the CrI<sub>3</sub> (WSe<sub>2</sub>) layer are labeled by solid (dashed) arrows.

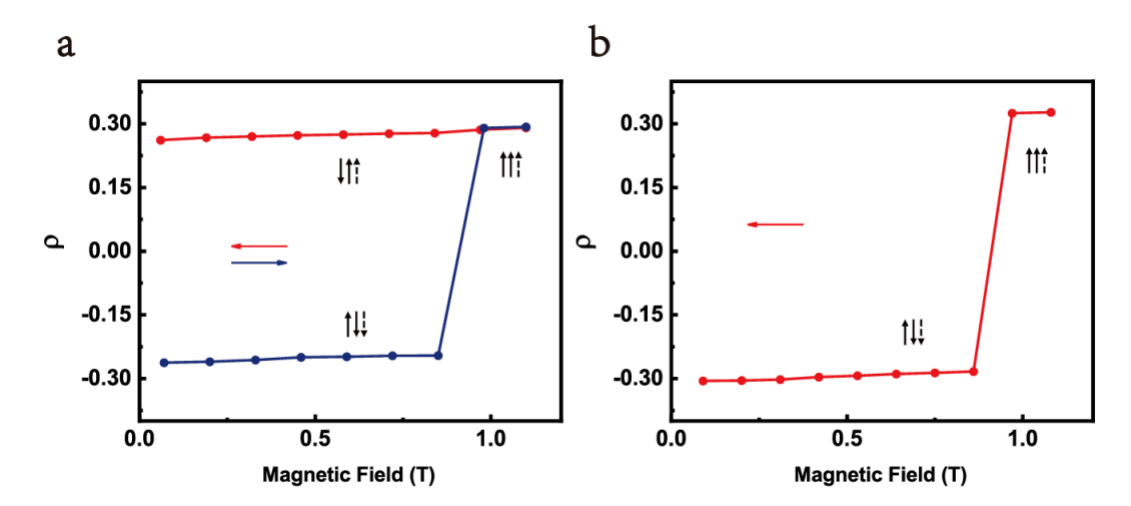


Figure 3(a) Spectrally integrated PL handedness  $\rho$  as a function of magnetic field near the spin-flip transition for WSe<sub>2</sub> coupled to the hard CrI<sub>3</sub> layer in a WSe<sub>2</sub>-bilayer CrI<sub>3</sub> heterostructure. The PL handedness can only be switched once as the magnetic field increases beyond the spin-flip transition field (blue). The PL handedness remains almost unchanged in the reverse scanning direction (red). The spin directions of the CrI<sub>3</sub> (WSe<sub>2</sub>) layer are labeled by solid (dashed) arrows. (b) Same as (a) for a different device with WSe<sub>2</sub> coupled to the soft CrI<sub>3</sub> layer. After the sample magnetization of CrI<sub>3</sub> is saturated at 1.1 T, the PL handedness can be switched back to the original state at the spin-flip transition.

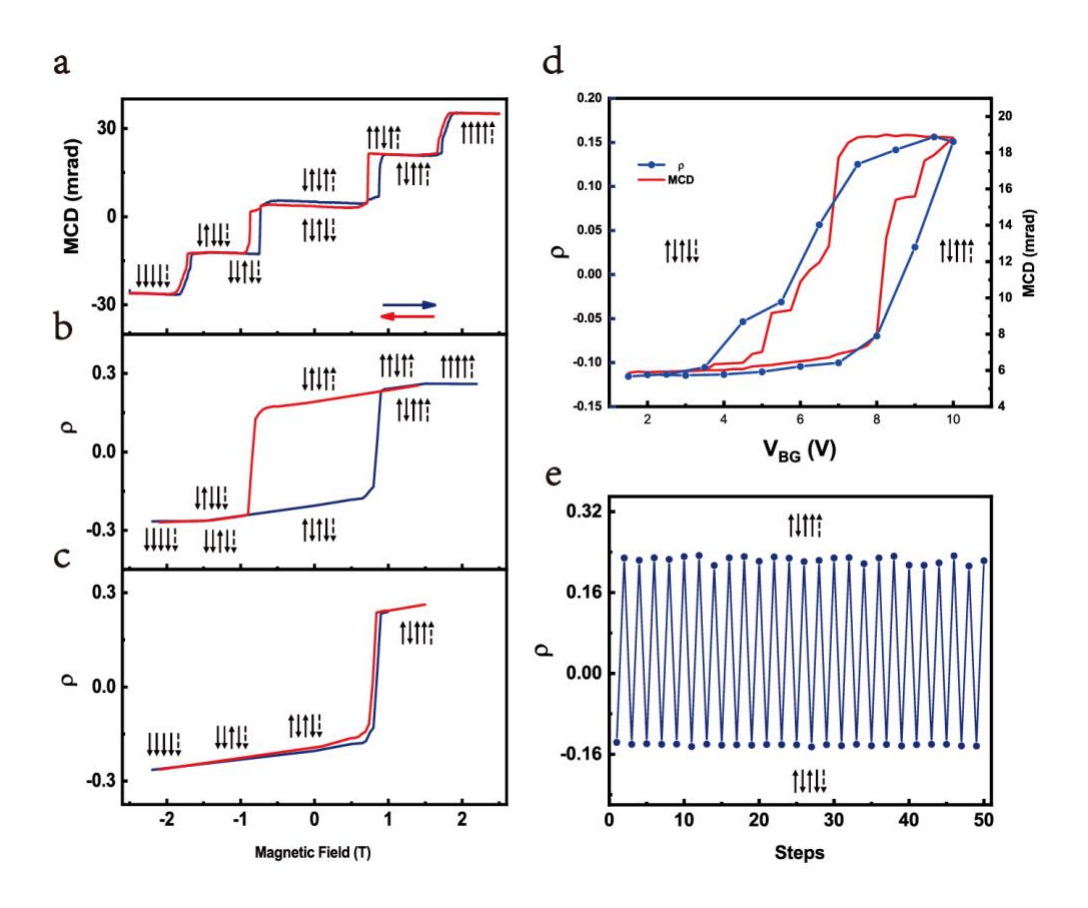


Figure 4. MCD (a), PL handedness  $\rho$  (b and c) as a function of magnetic field for a monolayer WSe<sub>2</sub>/4-layer CrI<sub>3</sub> device. The spin directions of the CrI<sub>3</sub> (WSe<sub>2</sub>) layer are labeled by solid (dashed) arrows. The magnetic field is scanned in the full range between -2.2 T and +2.2 T in (b), and is scanned between -2.2 T and +1.5 T in (c). Sign change in the PL handedness is seen only for the spin-flip transitions of the CrI<sub>3</sub> surface layers. (d) Integrated PL handedness (blue) and MCD (red) as a function of  $V_{BG}$  at 0.7 T and  $V_{TG} = 3$  V. Reversible electrical switching of PL handedness is seen. (e) Corresponding electrical switching of the PL handedness for 20 cycles as  $V_{BG}$  is switched between 0 V and 10 V.